

O-GlcNAc glycosylation orchestrates fate decision and niche function of bone marrow stromal progenitors

Zengdi Zhang^{1†}, Zan Huang^{1,2,3†}, Mohamed Awad⁴, Mohammed Elsalanty⁴, James Cray⁵, Lauren E Ball⁶, Jason C Maynard⁷, Alma L Burlingame⁷, Hu Zeng^{8,9}, Kim C Mansky¹⁰, Hai-Bin Ruan^{1,11*}

¹Department of Integrative Biology and Physiology, University of Minnesota Medical School, Minneapolis, United States; ²Laboratory of Gastrointestinal Microbiology, Jiangsu Key Laboratory of Gastrointestinal Nutrition and Animal Health, College of Animal Science and Technology, Nanjing Agricultural University, Nanjing, China; ³National Center for International Research on Animal Gut Nutrition, Nanjing Agricultural University, Nanjing, China; ⁴Department of Medical Anatomical Sciences, College of Osteopathic Medicine of the Pacific, Western University of Health Sciences, Pomona, United States; ⁵Department of Biomedical Education and Anatomy, The Ohio State University College of Medicine, and Division of Biosciences, The Ohio State University College of Dentistry, Columbus, United States; ⁶Department of Cell and Molecular Pharmacology & Experimental Therapeutics, Medical University of South Carolina, Charleston, United States; ⁷Department of Pharmaceutical Chemistry, University of California, San Francisco, San Francisco, United States; ⁸Division of Rheumatology, Department of Internal Medicine, Mayo Clinic, Rochester, United States; ⁹Department of Immunology, Mayo Clinic, Rochester, United States; ¹⁰Department of Developmental and Surgical Sciences, School of Dentistry, University of Minnesota, Minneapolis, United States; ¹¹Center for Immunology, University of Minnesota Medical School, Minneapolis, United States

*For correspondence:

hruan@umn.edu

†These authors contributed equally to this work

Competing interest: The authors declare that no competing interests exist.

Funding: See page 17

Received: 08 December 2022

Preprinted: 21 December 2022

Accepted: 01 March 2023

Published: 02 March 2023

Reviewing Editor: Yunlei Yang, Albert Einstein College of Medicine, United States

© Copyright Zhang, Huang et al. This article is distributed under the terms of the [Creative Commons Attribution License](https://creativecommons.org/licenses/by/4.0/), which permits unrestricted use and redistribution provided that the original author and source are credited.

Summary In mammals, interactions between the bone marrow (BM) stroma and hematopoietic progenitors contribute to bone-BM homeostasis. Perinatal bone growth and ossification provide a microenvironment for the transition to definitive hematopoiesis; however, mechanisms and interactions orchestrating the development of skeletal and hematopoietic systems remain largely unknown. Here, we establish intracellular O-linked β -N-acetylglucosamine (O-GlcNAc) modification as a post-translational switch that dictates the differentiation fate and niche function of early BM stromal cells (BMSCs). By modifying and activating RUNX2, O-GlcNAcylation promotes osteogenic differentiation of BMSCs and stromal IL-7 expression to support lymphopoiesis. In contrast, C/EBP β -dependent marrow adipogenesis and expression of myelopoietic stem cell factor (SCF) is inhibited by O-GlcNAcylation. Ablating O-GlcNAc transferase (OGT) in BMSCs leads to impaired bone formation, increased marrow adiposity, as well as defective B-cell lymphopoiesis and myeloid overproduction in mice. Thus, the balance of osteogenic and adipogenic differentiation of BMSCs is determined by reciprocal O-GlcNAc regulation of transcription factors, which simultaneously shapes the hematopoietic niche.

Editor's evaluation

Bone marrow stromal cells (BMSCs) can differentiate into a variety of cell types such as osteoblasts, chondrocytes, and adipocytes. The authors of this important study provide compelling and strong evidence that ablating O-GlcNAc transferase (OGT) in BMSCs impairs bone formation but promotes marrow adiposity. The results show that the balance of osteogenic and adipogenic differentiation of BMSCs is controlled by reciprocal O-GlcNAc regulation of lineage-specifying transcription factors, and highlights the importance of an intracellular glycosylation process of specific proteins in establishing the BM niche for hematopoiesis.

Introduction

Mammalian bones support body structure, protect vital organs, and allow body movement. In addition, they provide an environment for hematopoiesis in the bone marrow (BM). Most bones in mammals are formed through endochondral ossification, which is initiated by mesenchymal condensation, followed by the differentiation of chondrocytes and perichondrial progenitors (*Kobayashi and Kronenberg, 2021*). Perichondrial progenitors expressing Osterix (encoded by the *Sp7* gene) co-migrate with blood vessels into the primary ossification center, giving rise to osteoblasts and transient stromal cells in the nascent BM cavity (*Chen et al., 2014; Liu et al., 2013; Maes et al., 2010; Mizoguchi et al., 2014*). At the perinatal stage, Osterix⁺ progenitors contribute to osteo-lineages and long-lived BM stromal cells (BMSCs) that exhibit trilineage differentiation potential into osteocytes, chondrocytes, and adipocytes.

The decision of BMSC fate is controlled by a transcriptional network of pro-osteogenic and anti-adipogenic transcription factors that pre-establishes osteogenic enhancers in BMSCs for rapid bone formation (*Rauch et al., 2019*). RUNX family transcription factor 2 (RUNX2), by regulating osteogenic genes including *Sp7*, determines the osteoblast lineage from the multipotent BMSCs. Mice with *Runx2* mutations completely lack skeletal ossification and die of respiratory failure (*Komori et al., 1997*). *Runx2*-haploinsufficient mice show specific skeletal abnormalities characteristic of human cleidocranial dysplasia (CCD), including persistent fontanels, delayed closure of cranial sutures, rudimentary clavicles, and dental abnormalities (*Otto et al., 1997; Takarada et al., 2016*). On the other hand, adipogenesis is driven by downregulation of pro-osteogenic factors, remodeling of the chromatin, and activation of adipogenic transcription factors, such as C/EBPs and PPAR γ (*Aaron et al., 2021; Rauch et al., 2019*). BM adiposity is associated with bone loss in osteoporosis caused by aging, menopause, and anorexia nervosa (*Bethel et al., 2013; Fazeli et al., 2013; Liu et al., 2015; Scheller et al., 2016*). However, it is incompletely understood how these distinct types of transcription factors act cooperatively to determine lineage differentiation during neonatal skeletal development.

BMSCs and their lineage-differentiated progeny (e.g. osteoblasts and adipocytes) provide a niche microenvironment for hematopoiesis (*Bianco and Robey, 2015; Calvi and Link, 2015; Morrison and Scadden, 2014; Wei and Frenette, 2018*). Recent studies using single-cell technologies and lineage tracing experiments have started to unveil the complexity and heterogeneity of niche cell types, niche factors, and their actions. For example, BMSC-derived stem cell factor (SCF, encoded by the *Kitl* gene) and CXC chemokine ligand 12 (CXCL12) are required for the maintenance and differentiation of hematopoietic stem/progenitor cells (HSPCs) (*Asada et al., 2017; Ding et al., 2012*). A prominent subpopulation of perivascular BMSCs express adipocyte markers (*Dolgalev and Tikhonova, 2021; Zhong et al., 2020; Zhou et al., 2017*), and support steady-state and metabolic-stressed myelopoiesis by secreting SCF (*Zhang et al., 2019*). Meanwhile, osteolineage cells are crucial for lymphopoiesis (*Wei and Frenette, 2018*). Depleting Osterix⁺ cells halts B cell maturation and causes immune failure (*Yu et al., 2016*). IL-7, the most crucial factor for lymphoid progenitors, is expressed by a subset of BMSCs (*Fistonich et al., 2018*). While it is well accepted that myeloid and lymphoid progenitors may reside in distinct BM niches, it is unclear how BMSC heterogeneity is established during early development and whether cytokine expression is coordinated and controlled by the fate-defining transcriptional network in BMSCs.

Post-translational modifications (PTMs), including phosphorylation, acetylation, and ubiquitination, allow the precise regulation of stability, localization, and activity of BM transcriptional factors, such as RUNX2 (*Chen et al., 2021; Kim et al., 2020*), C/EBPs (*Wang et al., 2022*), and PPAR γ (*Brunmeir and Xu, 2018*). It remains poorly defined how these modifications are coordinated in a spatio-temporal

manner to calibrate skeletal development. Thousands of intracellular proteins are dynamically modified by a single O-linked N-Acetylglucosamine (O-GlcNAc) moiety at serine or threonine residues, termed O-GlcNAcylation (Hart et al., 2007; Ruan et al., 2013b; Yang and Qian, 2017). O-GlcNAc transferase (OGT), using UDP-GlcNAc derived from the hexosamine biosynthetic pathway as the substrate, controls diverse biological processes such as gene transcription, protein stability, and cell signaling (Hanover et al., 2012; Ruan et al., 2014; Ruan et al., 2012; Ruan et al., 2013a). In cell culture, O-GlcNAcylation promotes osteogenesis (Kim et al., 2007; Nagel and Ball, 2014) and suppresses adipogenesis (Ji et al., 2012). However, the physiological relevance of O-GlcNAcylation in skeletal development and remodeling has not been established. Here, we studied OGT in balancing osteogenic versus adipogenic programs and in controlling niche function of BMSC in mice. The multifaceted role of protein O-GlcNAcylation is achieved through reciprocal regulation of pro-osteogenic, pro-lymphopoietic RUNX2 and pro-adipogenic, pro-myelopoietic C/EBP β .

Results

Loss of OGT in perinatal BMSCs leads to bone loss

To determine the *in vivo* role of protein O-GlcNAcylation in bone development, we deleted the X Chromosome-located *Ogt* gene using the *Sp7^{GFP:Cre}* mice (Figure 1A). Floxed *Ogt^{f/f}* were bred with *Sp7^{GFP:Cre}* to generate *Ogt* conditional knockout (cKO) mice. Compared to *Sp7^{GFP:Cre}* littermate controls, newborn *Ogt* cKO mice showed no obvious change in long bone formation (Figure 1B) but had a profound defect in the mineralization of flat bones of the calvaria (Figure 1C), suggesting impaired intramembranous ossification during the prenatal stage.

At 4–6 weeks of age, *Ogt* cKO mice were modestly shorter than the controls (Figure 1D and E). Histological analyses showed decreased bone volume and osteoblast number (Figure 1F) and shortened growth plate (Figure 1G) in *Ogt* cKO mice. Micro-CT scanning further showed that *Ogt* cKO mice had reduced trabecular bone volume, bone volume to tissue volume ratio, trabecular thickness, and trabecular numbers in the distal femur (Figure 1H–L). *Ogt* cKO mice represent typical bone and dental defects (Figure 1—figure supplement 1) as observed in *Runx2*-haploinsufficient mice (Otto et al., 1997; Takarada et al., 2016), suggesting that O-GlcNAcylation might control RUNX2 function. Moist food was provided to these animals after weaning to prevent malnutrition.

RUNX2 O-GlcNAcylation promotes osteogenesis

To investigate how OGT controls osteogenic differentiation of BMSCs, we first isolated primary BMSCs from control and *Ogt* cKO mice and induced them into osteoblast cells. Alkaline phosphatase staining revealed a reduction in mineralization of *Ogt* cKO BMSCs (Figure 2A). Similarly, treating mesenchymal C3H10T1/2 cells with an OGT inhibitor, OSMI-1, reduced mineralization (Figure 2B) and ablated calcium deposition (Figure 2C) after osteogenic differentiation. Parathyroid hormone (PTH) is a bone anabolic agent that requires RUNX2-dependent signaling (Krishnan et al., 2003). We found that PTH treatment of C3H10T1/2 cells increased global protein O-GlcNAcylation (Figure 2D). The ability of PTH to activate osteogenesis is completely abolished when OGT was inhibited by OSMI-1 (Figure 2E). Pharmacological activation of O-GlcNAcylation enhances RUNX2 activity and promotes osteogenic differentiation (Kim et al., 2007; Nagel and Ball, 2014). We mutated three known O-GlcNAc sites on RUNX2, Ser 32 and Ser 33 in the N-terminal transactivation domain and Ser 371 in the proline/serine/threonine-rich domain (Figure 2F), to alanine (3A), and found that mutant RUNX2 possessed less O-GlcNAcylation (Figure 2G). O-GlcNAcase (OGA) inhibition by Thiamet-G (TMG) increased O-GlcNAcylation of wildtype (WT) RUNX2, but to a much less extent in the 3A mutant (Figure 2G). OGT inhibition by OSMI-1 or O-GlcNAc mutation both impaired the transcriptional activity of RUNX2 on a luciferase reporter (Figure 2H). OSMI-1 could still suppress of luciferase activity of RUNX2-3A (Figure 2H), suggesting additional, unidentified O-GlcNAc sites (Figure 2G), which requires future investigation. Nevertheless, when overexpressed in C3H10T1/2 cells, RUNX2-3A substantially lost the ability to induce osteogenic differentiation (Figure 2I) or RUNX2-target gene expression (Figure 2J). These data demonstrate that O-GlcNAcylation is essential for RUNX2 activity and osteogenesis.

In adult mice, *Sp7* expression is restricted to osteoblast precursors. We treated *Ogt* cKO mice from pregnancy with doxycycline (Dox) and withdrew Dox at 10 weeks of age to induce Cre expression and OGT depletion only during adulthood (Figure 3A). Micro-CT showed that *Ogt* cKO mice had reduced

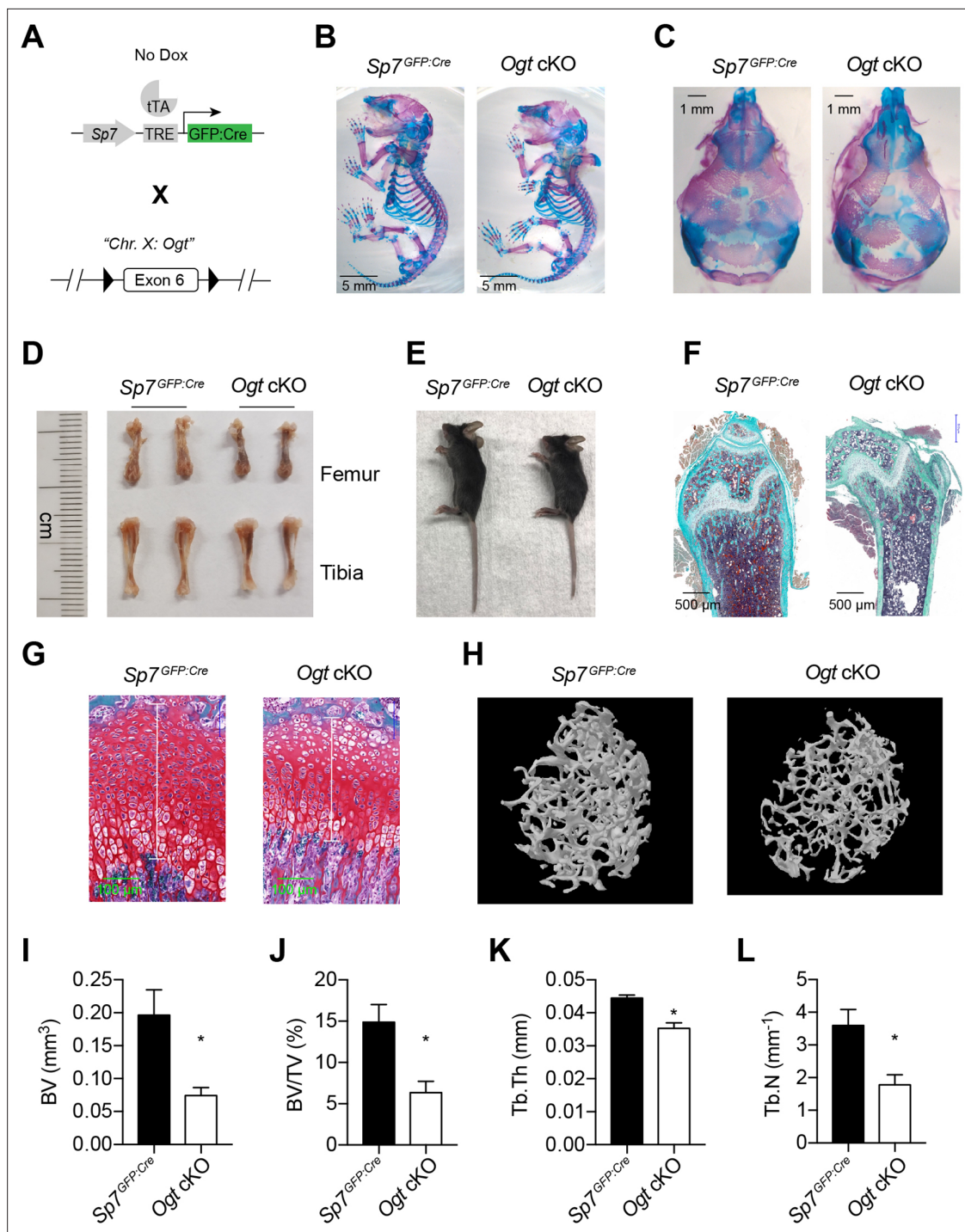


Figure 1. Impaired osteogenesis in *Ogt* cKO mice. **(A)** Mating strategy to generate *Ogt* cKO mice. Note that the *Ogt* gene is located on Chr. X, thus males are hemizygous *Ogt*^{fl/y}. **(B, C)** Whole mount Alizarin red and Alcian blue staining of newborn mice. **(D, E)** Long bone length **(D)** and gross morphology of 4–6 weeks old mice. **(F, G)** Goldner's trichrome **(F)** and Safranin O **(G)** staining of femurs from 4-week-old mice. **(H–L)** Micro-CT of 6-week-old mice **(H, n=3–4)**. Bone volume (BV, **I**), BV/tissue volume ratio (BV/TV, **J**), trabecular thickness (Tb.Th, **K**), and trabecular number (Tb.N, **L**) were calculated. Data are presented as mean ± SEM. *, p<0.05 by unpaired student's *t*-test.

The online version of this article includes the following figure supplement(s) for figure 1:

Figure supplement 1. Dental defects of *Ogt* cKO mice.

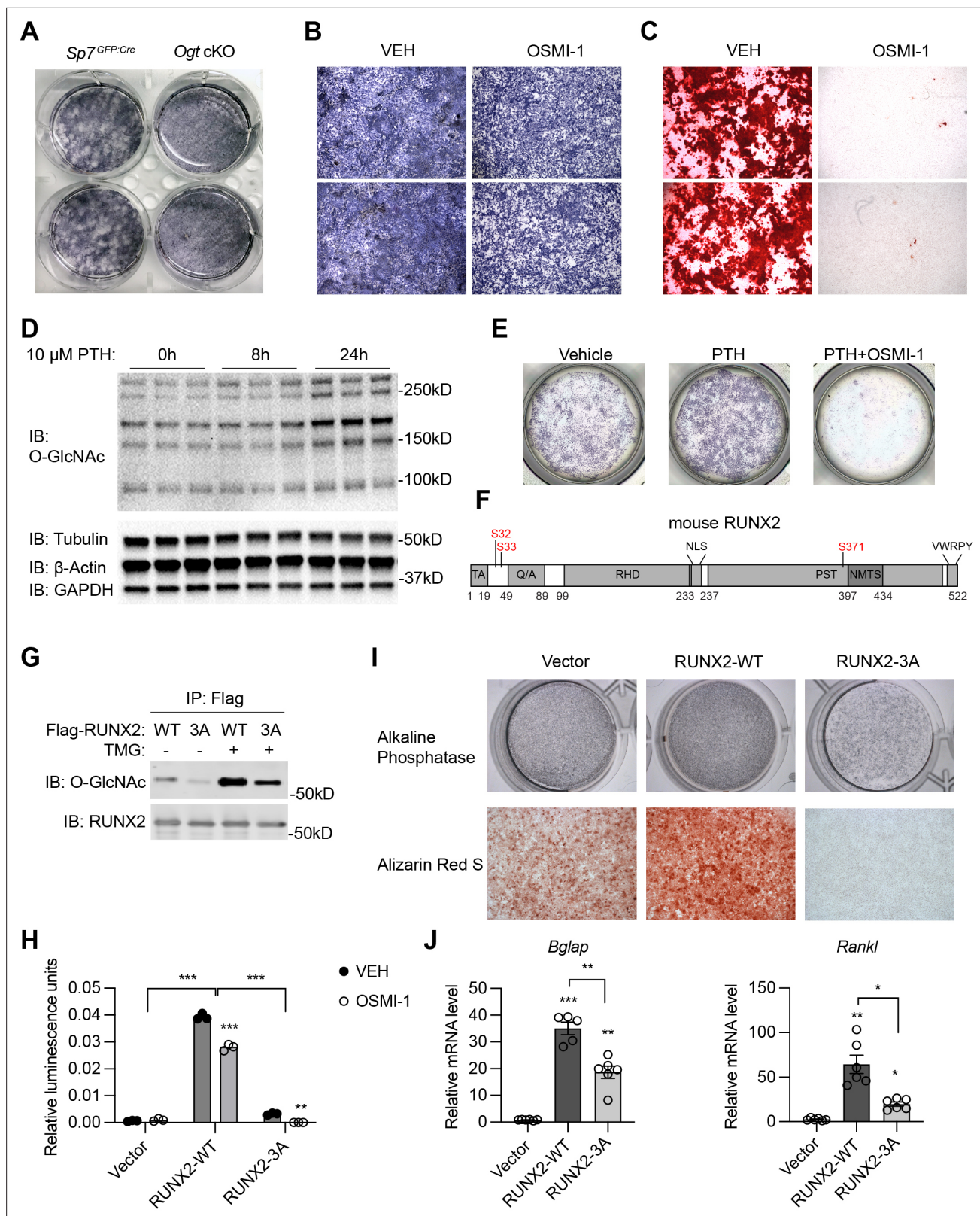


Figure 2. RUNX2 O-GlcNAcylation is required for osteogenesis. **(A)** Alkaline phosphatase (ALP) staining of control and *Ogt cKO* BMSCs differentiated to the osteogenic lineage. **(B, C)** Primary BMSCs, in the presence or absence of the OGT inhibitor OSMI-1, were induced for osteogenesis and stained for ALP **(B)** and Alizarin Red S **(C)**. **(D)** Primary BMSCs were treated with PTH for the indicated time and subjected to Western blotting of total protein O-GlcNAcylation. **(E)** BMSCs were treated with PTH alone or together with OSMI-1, osteogenic differentiated, and stained for ALP (n=3). **(G)** Flag-tagged *Figure 2 continued on next page*

Figure 2 continued

wildtype (WT) and O-GlcNAc mutant (3A) RUNX2 plasmids were overexpressed in HEK293 cells, and their O-GlcNAcylation was determined by Flag immunoprecipitation followed with O-GlcNAc western blot. (H) 6xOSE-luciferase activity in COS-7 cells transfected with WT or 3A-mutant RUNX2, in the presence or absence of the OGT inhibitor, OSMI-1. (I, J) C3H10T1/2 cells with lentiviral overexpression of RUNX2 were osteogenically differentiated and stained with ALP or Alizarin Red S (I). Expression of *Bglap* and *Rankl* was determined by RT-qPCR (J). Data are presented as mean \pm SEM. *, $p < 0.05$; **, $p < 0.01$; and ***, $p < 0.001$ by two-way ANOVA (H) or one-way ANOVA (J). Representative images from at least three biological replicates were shown in A, B, C, E, and I.

The online version of this article includes the following source data for figure 2:

Source data 1. Raw uncropped images for panel D.

Source data 2. Raw uncropped images for panel G.

bone volume, trabecular thickness, and bone mineral density (Figure 3B–E). Together, these results support the functional indispensability of OGT in the committed osteolineage for adult trabecular bone remodeling.

C/EBP β O-GlcNAcylation inhibits the adipogenic specification of BMSCs

The osteogenic and adipogenic differentiation of BMSCs is generally considered mutually exclusive (Ambrosi et al., 2017). Concomitant with bone loss, we observed a massive accumulation of adipocytes in the bone marrow of *Ogt* cKO mice, shown by hematoxylin & eosin staining (Figure 4A) and immune-staining of the lipid droplet protein – perilipin (Figure 4B). *Pdgfra* and *Vcam1* (encoding CD106) have been recently identified as surface markers of adipogenic lineage cells in the BM that also express the *Lepr* and *Adipoq* genes (Figure 4—figure supplement 1; Baryawno et al., 2019; Zhong et al., 2020). Flow cytometric analysis of BMSCs revealed that *Ogt* cKO mice possessed more PDGFR α ⁺VCAM1⁺ adipogenic progenitors than littermate controls (Figure 4C). To directly test if OGT deficiency biases BMSC differentiation toward the adipogenic lineage, we first induced the adipogenic differentiation of primary BMSCs and found increased lipid deposition in *Ogt* cKO mice (Figure 4D). Even under an osteogenic induction condition, adipo-lineage markers such as *Adipoq* and *Vcam1* were significantly upregulated by OGT deficiency (Figure 4E and F). Furthermore, treating C3H10T1/2 mesenchymal cells with an OGA inhibitor TMG to increase protein O-GlcNAcylation, was able to substantially reduce perilipin protein expression (Figure 4G) and *Pparg* and *Adipoq* gene expression (Figure 4H, I). These data indicate that OGT inhibits the adipogenic program of BMSCs.

We went on to determine the O-GlcNAc targets of OGT in suppressing adipogenesis. As an osteogenic regulator, RUNX2 also reciprocally suppresses the adipogenic program (Ahrends et al., 2014). However, such suppression was not dependent on O-GlcNAcylation, because O-GlcNAc-deficient RUNX2 displayed similar efficiency as the wildtype protein to reduce lipid deposition and perilipin expression in differentiated C3H10T1/2 cells (Figure 4—figure supplement 2). It is possible that O-GlcNAc on RUNX2 selectively facilitates the recruitment of transcriptional co-activators for

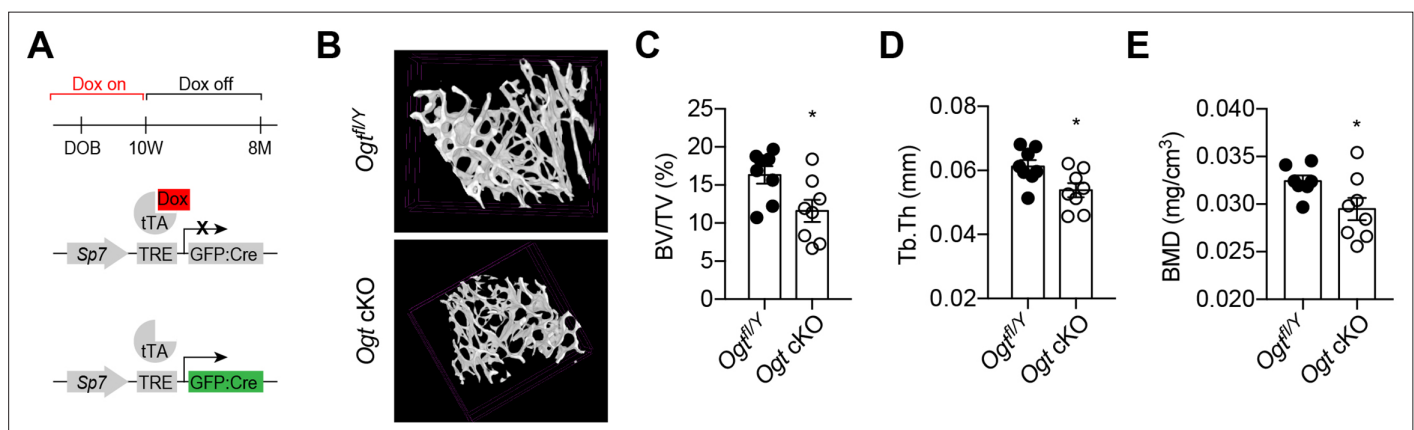


Figure 3. Adult-onset deletion of OGT impairs trabecular bone formation. (A) Dox treatment timeline in *Ogt* cKO to achieve osteoblast-specific deletion of OGT. (B–D) Micro-CT (B) showing reduced bone volume/tissue volume (C), trabecular thickness (D), and trabecular bone mineral density (E). Data are presented as mean \pm SEM. *, $p < 0.05$ by unpaired student's t-test.

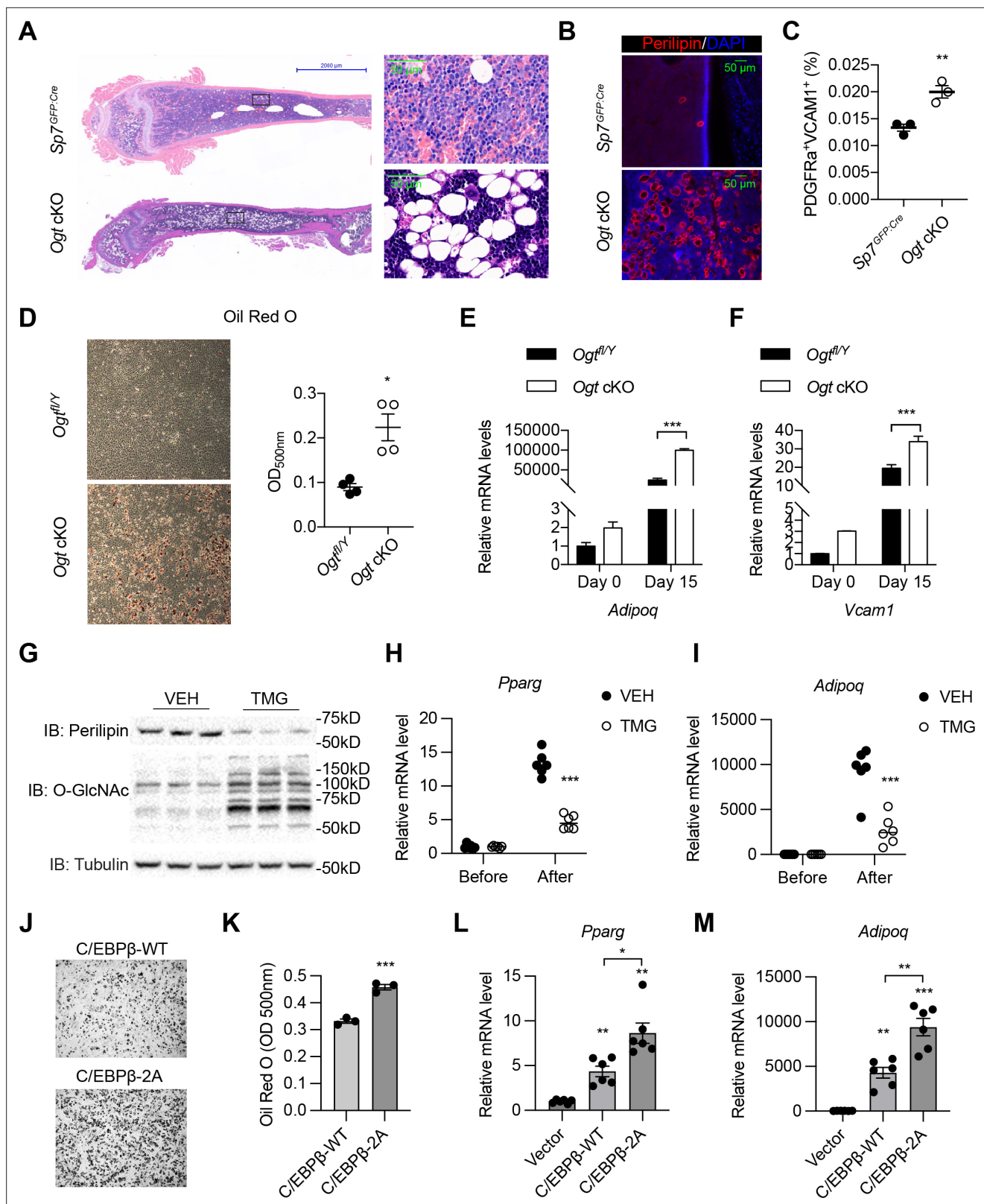


Figure 4. O-GlcNAcylation inhibits BM adipogenesis. (A, B) H&E (A) and Perilipin immunofluorescent staining (B) on femur sections from 4-week-old mice. (C) Flow cytometric quantification of PDGFRα⁺VCAM1⁺ preadipocytes frequencies within the live BM cells (n=3). (D) Adipogenic differentiation of primary BMSCs from control and *Ogt* cKO mice. Lipid was stained with Oil Red O and quantified to the right (n=4). (E, F) Primary BMSCs were osteogenic differentiated for 0 or 15 days. Expression of *Adipoq* (E) and *Vcam1* (F) genes was determined by RT-qPCR (n=3). (G-I) C3H10T1/2 cells, Figure 4 continued on next page

Figure 4 continued

treated with or without TMG, were adipogenic differentiated. Western blotting for perilipin and O-GlcNAc of differentiated cells (G) and RT-qPCR for adipogenic marker *Pparg* (H) and *Adipoq* (I) expression. (J–M) Adipogenic differentiation of C3H10T1/2 cells infected with lentiviral C/EBP β . Oil Red O was stained (J) and quantified (K). *Pparg* (L) and *Adipoq* (M) gene expression was determined by RT-qPCR. Data are presented as mean \pm SEM. *, $p < 0.05$; **, $p < 0.01$; and ***, $p < 0.001$ by unpaired student's t-test (C, D, K), one-way ANOVA (L, M), and two-way ANOVA (E, F, H, I).

The online version of this article includes the following source data and figure supplement(s) for figure 4:

Source data 1. Mass spectrometry search results of all protein modifications (Table S1) and PPAR γ 2 O-GlcNAc sites (Table S2).

Source data 2. Raw uncropped images for panel G.

Figure supplement 1. *Pdgra*⁺*Vcam1*⁺ cells as adipogenic progenitors.

Figure supplement 1—source data 1. Raw uncropped images for **Figure 4—figure supplement 1B**.

Figure supplement 2. RUNX2 inhibits adipogenesis independently of O-GlcNAcylation.

Figure supplement 3. PPAR γ 2 O-GlcNAcylation is required for adipogenesis.

osteogenesis but does not suppress the chromatin remodeling needed for the activation of adipogenic transcriptional factors.

PPAR γ 1 is O-GlcNAcylated at T54 in the A/B activation domain (Ji et al., 2012), corresponding to T84 in PPAR γ 2, the major isoform in adipocytes (Figure 4—figure supplement 3A). Mutating T84 in PPAR γ 2 did not ablate the ability of the OGA inhibitor TMG to suppress adipogenesis in C3H10T1/2 cells (data not shown), suggesting the existence of other unidentified O-GlcNAc sites on PPAR γ 2 or other target proteins than PPAR γ 2. Through mass spectrometry, we were able to map four additional O-GlcNAc sites on PPAR γ 2 (Figure 4—figure supplement 3A and Figure 4—source data 1). Intriguingly, mutating these four sites or together with T84 to alanine, render PPAR γ 2 incompetent to induce transcription and adipogenesis (Figure 4—figure supplement 3B, C). It suggests that PPAR γ 2 O-GlcNAcylation is essential for adipocyte maturation, but likely does not mediate the anti-adipogenic effect of OGT in perinatal BMSCs.

We then looked to C/EBP β , an early transcription factor that specifies the adipogenic fate of BMSCs (Cao et al., 1991; Darlington et al., 1998). It has been reported that OGT modifies C/EBP β to inhibit its transcriptional activity (Li et al., 2009; Qian et al., 2018). As expected, ablating O-GlcNAcylation of C/EBP β (2A mutation) promotes adipogenic differentiation of C3H10T1/2 cells (Figure 4J and K). Taken together, we concluded that, by O-GlcNAcylation and reciprocally regulating RUNX2 and C/EBP β , OGT is required for the proper allocation of skeletal progenitors into osteogenic versus adipogenic lineages during development.

OGT deficiency disrupts the BM niche

Skeletal development is concomitant with the establishment of definitive hematopoiesis in the BM. To test if OGT deficiency affects the niche function of *Sp7*⁺ cells for B-cell lymphopoiesis, we performed flow cytometry analyses of bone marrow of 4-week-old mice (Figure 5A, Figure 5—figure supplement 1 and Figure 5—source data 1; Hardy et al., 1991). No changes in the percentage of lineage Sca-1⁺Kit⁺ (LSK) progenitor cells, common lymphoid progenitors (CLPs), Fraction A that contains pre-pro-B cells were observed between control and *Ogt* cKO mice (Figure 5B–D). While frequencies of Fraction B and C pro-B, pre-B, and immature B in *Ogt* cKO mice were drastically reduced (Figure 5E–I), demonstrating a developmental blockage from pre-pro-B to pro-B cells. In the peripheral blood, there was specific loss of CD19⁺B220⁺ B cells but not CD4⁺ or CD8⁺ T cells (Figure 5J–L). B-cell dysfunction observed here was similar to the phenotype in mice when all *Sp7*⁺ cells were depleted (Yu et al., 2016) or IL-7 was deleted in BMSCs (Cordeiro Gomes et al., 2016), indicating that O-GlcNAcylation is essential for the *Sp7*⁺ lineage cells to establish a niche environment for B-cell lymphopoiesis.

BM adiposity is associated with myeloid overproduction in conditions including aging, irradiation (Ho et al., 2019), osteopenia (Kajkenova et al., 1997), and obesity (Singer et al., 2014), indicating the supportive function of marrow adipocytes on demand-adapted myelopoiesis. Consistently with the increased BM adiposity found in *Ogt* cKO mice, we also observed biased HSPC differentiation toward the myeloid lineage, as shown by increased ratio of common myeloid progenitor (CMP) to common lymphoid progenitors (CLPs) and ratio of granulocyte-monocyte progenitors (GMP) to megakaryocyte-erythrocyte progenitors (MEP) in the BM (Figure 5M and N). As a result, increased numbers of red blood cells and neutrophils were observed in the blood of *Ogt* cKO mice (Figure 5O

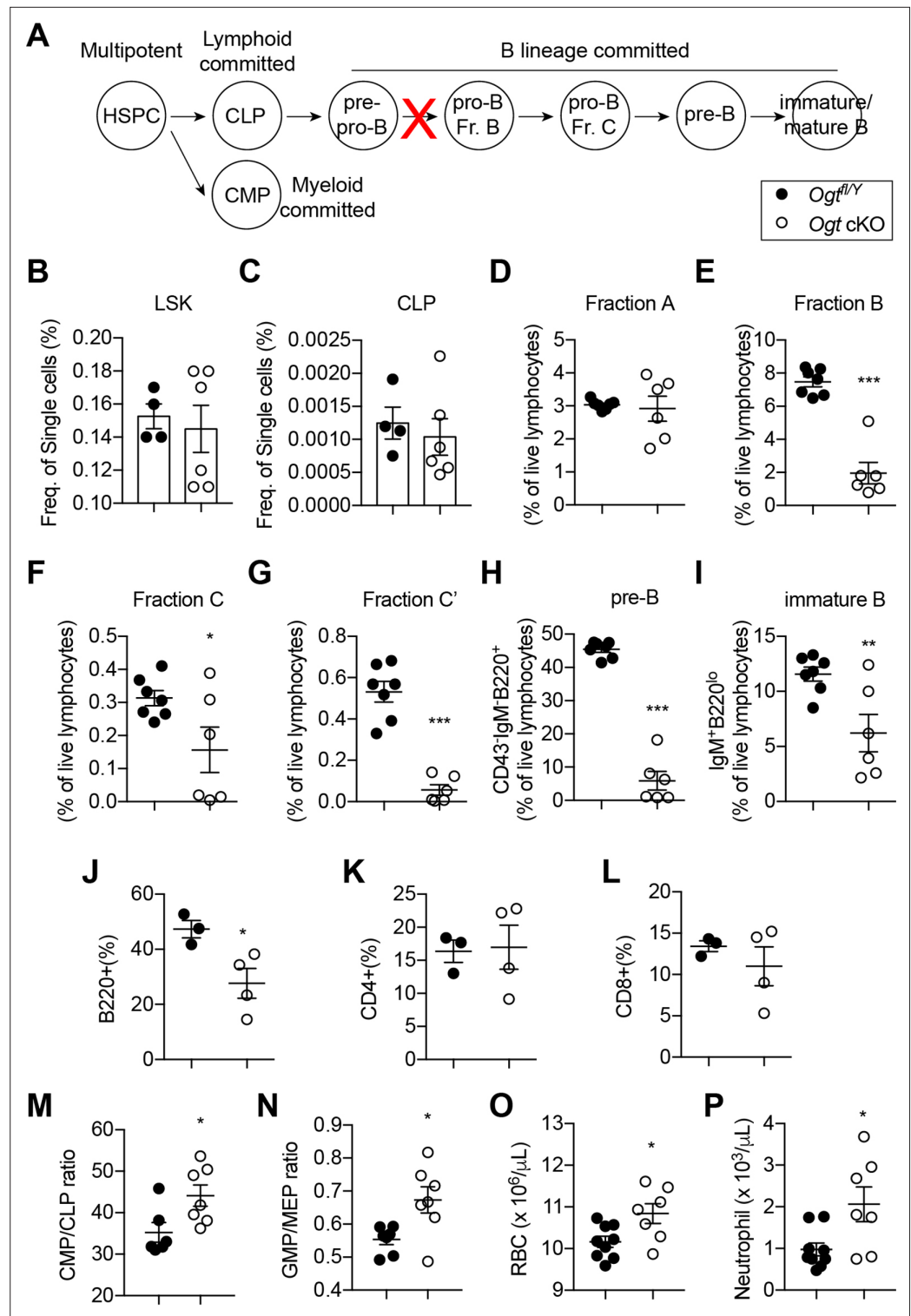


Figure 5. Impaired B lymphopoiesis and myeloid skewing in *Ogt cKO* mice. (A) Schematic view of B cell development in the BM and blockade by stromal OGT deficiency (red X). (B–C) Flow cytometric quantification of LSK (B) and CLP (C) among live BM cells (n=4–6). (D–I) Flow cytometric quantification of fraction A (D), fraction B (E), fraction C (F), fraction C' (G), fraction D (H), and immature B (I) frequencies among live BM lymphocytes (n=6–7). (J–L) Flow cytometric quantification of B220⁺ B cell (J), CD4⁺ T cell (K), and CD8⁺ T cell (L) percentages in the blood (n=3–4). (M, N) CMP/CLP ratio (M) and GMP/IEP ratio (N) in the BM (n=6–7). (O, P) Complete blood

Figure 5 continued on next page

Figure 5 continued

counting showing numbers of RBC (O) and neutrophil (P) (n=7–9). Data are presented as mean ± SEM. *, p<0.05; **, p<0.01; and ***, p<0.001 by unpaired student's t-test.

The online version of this article includes the following source data and figure supplement(s) for figure 5:

Source data 1. Antibodies used for flow cytometry.

Figure supplement 1. Flow cytometry of BM B cells.

and P). Together, these results demonstrate that OGT deficiency in neonatal BMSCs establishes a BM environment that promotes myelopoiesis and simultaneously impairs B cell development.

Transcriptional regulation of niche cytokines by RUNX2 and C/EBPβ O-GlcNAcylation

BMSC-derived SCF (encoded by the *Kitl* gene) and IL-7 are required for the myeloid differentiation and B-cell development, respectively (Asada et al., 2017; Cordeiro Gomes et al., 2016; Ding et al., 2012). We sought to test if their expression is controlled by the same transcriptional network determining BMSC fate. Adipogenic differentiation of mesenchymal C3H10T1/2 cells concomitantly increased *Kitl* while decreased *Il7* gene expression (Figure 6A and B). Simultaneous treatment with the OGT inhibitor OSMI-1 dampened *Il7* expression before differentiation but enhanced *Kitl* expression in differentiated adipocytes (Figure 6A and B). On the other hand, osteogenic differentiation suppressed *Kitl* transcription, which could be further inhibited by TMG that elevated global O-GlcNAcylation (Figure 6C). While *Il7* mRNA levels were not evidently affected by osteogenic differentiation, TMG stimulated its expression (Figure 6D). O-GlcNAcylation inhibits the adipogenesis specified by C/EBPβ but supports osteogenesis determined by RUNX2. In concert, C/EBPβ overexpression in C3H10T1/2 cells activated *Kitl* transcription and suppressed *Il7* expression, which was further

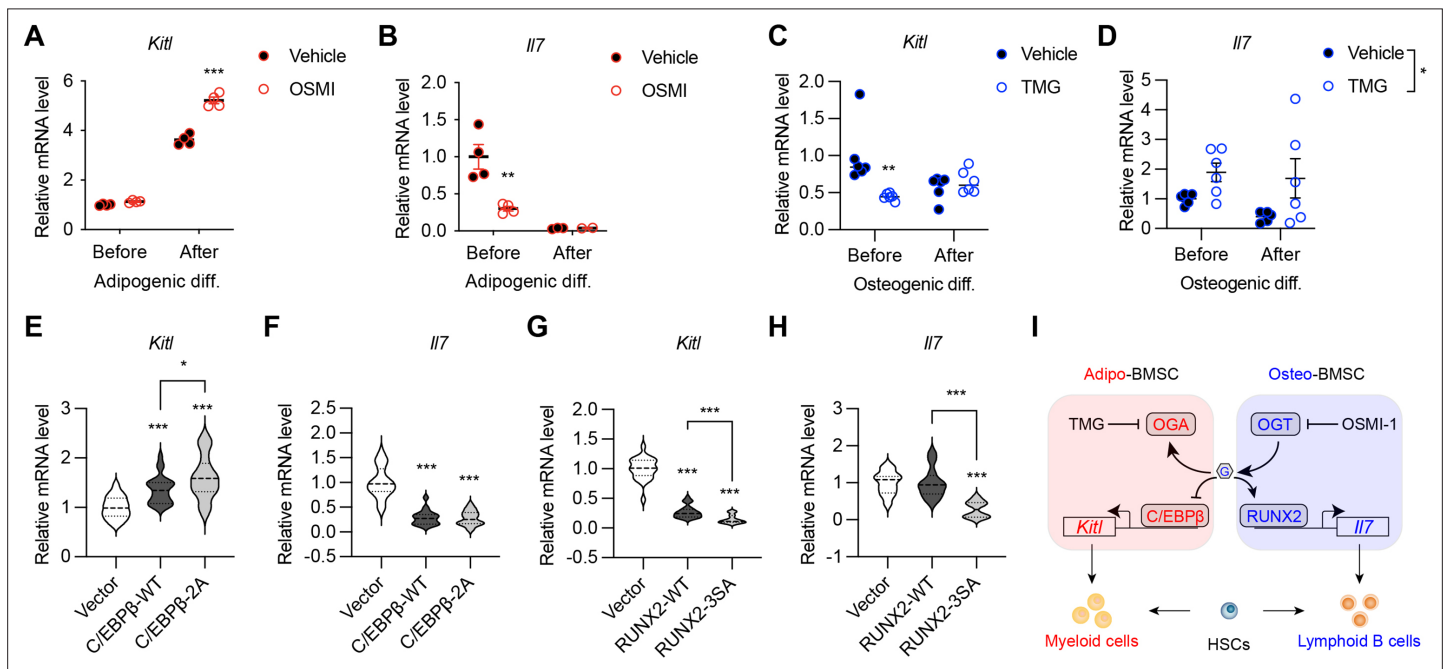


Figure 6. O-GlcNAc regulation of niche cytokine expression. (A, B) C3H10T1/2 cells were treated with vehicle or OGT inhibitor OSMI and differentiated for adipocytes (n=4). *Kitl* (A) and *Il7* (B) gene expression was determined by RT-qPCR. (C, D) C3H10T1/2 cells were treated with vehicle or OGA inhibitor TMG and induced for osteogenic differentiation (n=6). *Kitl* (C) and *Il7* (D) gene expression was determined by RT-qPCR. (E–H) C3H10T1/2 cells were infected with lentiviruses expressing WT and O-GlcNAc-deficient C/EBPβ (E, F) or RUNX2 (G, H). Expression *Kitl* (E, G) and *Il7* (F, H) was measured by RT-qPCR (n=6). (I) Proposed action of protein O-GlcNAcylation in regulating the BMSC niche function. Data are presented as mean ± SEM. *, p<0.05; **, p<0.01; ***, p<0.001 by two-way ANOVA (A–D) and one-way ANOVA (E–H).

The online version of this article includes the following source data for figure 6:

Source data 1. Sequences of oligos used for RT-qPCR.

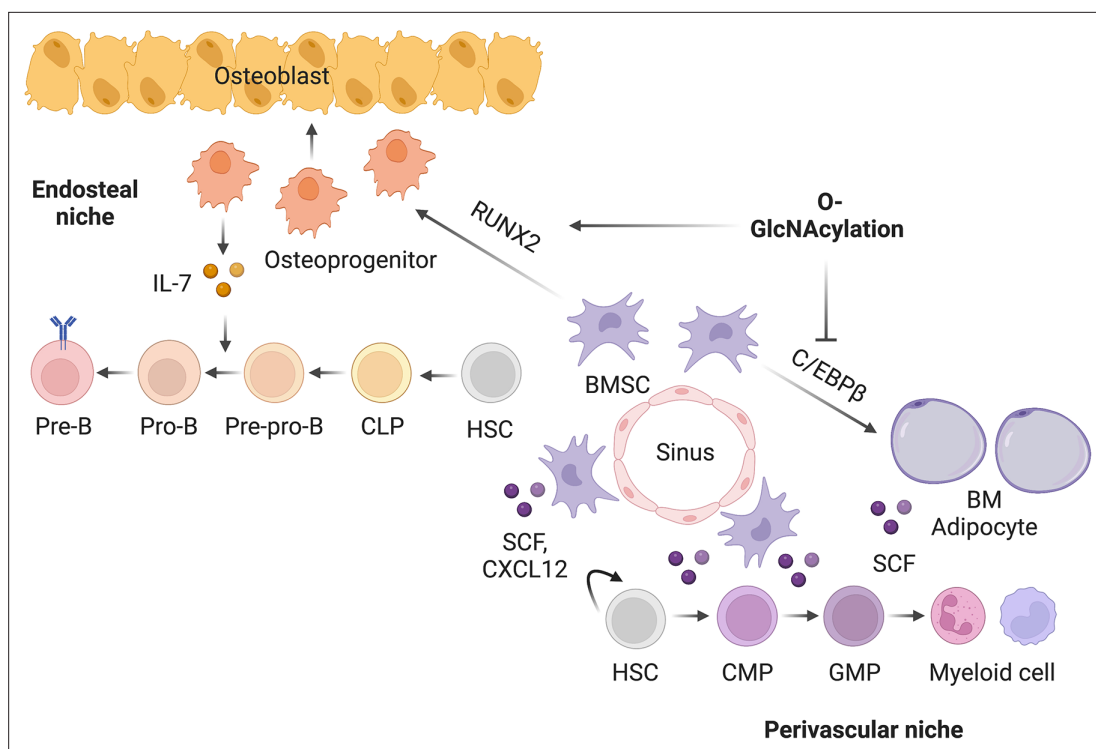


Figure 7. Working model of O-GlcNAc signaling in bone-BM development.

exacerbated by O-GlcNAc-deficient C/EBP β (**Figure 6E and F**). However, RUNX2 overexpression decreased *Kitl* mRNA levels (**Figure 6G**). When compared to the wildtype, O-GlcNAc-defective RUNX2 was impaired in inducing *Ilf7* expression (**Figure 6H**). Collectively, these results reveal that protein O-GlcNAcylation, by acting on BMSC lineage transcriptional factors, establishes a pro-lymphopoietic niche during neonatal bone development and at the same time prevents the myeloid-skewing, adipogenic BM environment.

Discussion

Post-translational modification networks exist in the bone-BM organ to regulate its development and remodeling. Given that definitive hematopoiesis is matured in perinatal BM, it is tempting to hypothesize that the regulatory mechanisms guiding the development of bone also establish the BM niche for hematopoiesis. However, experimental evidence has been largely lacking so far. In the present study, we examined the vital role of the under-studied protein O-GlcNAcylation in determining the osteogenic versus adipogenic fate specification of BMSCs and in balancing the pro-lymphopoietic and pro-myelopoietic niche function of BMSCs. We showed that, by modifying and reciprocally regulating RUNX2 and C/EBP β , O-GlcNAc orchestrates the early development of skeletal and hematopoietic systems (**Figure 7**).

Multiple temporally and spatially distinct types of progenitors contribute to bone development and maintenance. In the early embryo, *Sp7*⁺ progenitors give rise to fetal bone tissues and transient stromal cells that disappear in early postnatal life (**Mizoguchi et al., 2014**). Perinatally, *Sp7*⁺ progenitors contribute to osteolineage cells and long-lived perivascular BMSCs that can be labeled by leptin receptor (*LepR*) and adiponectin (*Adipoq*) (**Zhong et al., 2020; Zhou et al., 2017**). Recent evidence suggests that a significant portion of adult BMSCs and osteoblasts originate from collagen II (*Col2*)- and aggrecan (*Acan*)-expressing chondrocytes (**Ono et al., 2014**). Due to the fact that *Sp7*^{GFP:Cre} targets osteoblasts, BMSCs, and a subset of chondrocytes (**Chen et al., 2014; Liu et al., 2013**), the current study could not delineate the exact developmental stages and the primary cellular compartments where OGT instructs bone development. Nonetheless, our ex vivo experiments and adult-onset targeting of OGT in *Sp7*⁺ osteoblasts, together with prior published in vivo and in vitro

evidence (Andrés-Bergós *et al.*, 2012; Nagel and Ball, 2014; Nagel *et al.*, 2013), certainly reveal the indispensability of protein O-GlcNAcylation for chondro-osteogenic differentiation. While this study primarily focused early life bone development, it is warranted to further investigate the role of OGT in the transition to appositional remodeling during adulthood (Shu *et al.*, 2021) and in osteoporosis pathogenesis during aging. Moreover, bone-forming skeletal stem cells (SSCs) are identified in other anatomical regions of long bones, such as growth plate, periosteum, and endosteum (Ambrosi *et al.*, 2019). It remains undetermined whether O-GlcNAcylation is abundant in and controls the development and function of these SSC populations.

O-GlcNAcylation is required for PPAR γ to drive adipogenesis, but why did not OGT-deficient BMSCs arrest their differentiation after being committed to the adipogenic lineage. One speculation is that PPAR γ O-GlcNAcylation is extremely low in homeostatic conditions, which might help explain the rare appearance of adipocytes in young BM. If so, the loss of PPAR γ O-GlcNAcylation in *Ogt* cKO mice would not block adipogenesis. Second, the differentiation of marrow adipose tissue (MAT) is distinct from peripheral white adipose tissue (WAT). For instance, adipogenic BMSCs in adult mice already express large amount of *Adipoq*, which is only present in mature WAT adipocytes. Certain forms of genetic lipodystrophy (e.g. mutations in *CAV1* and *PTRF*) selectively lose peripheral WAT but preserve MAT (Scheller *et al.*, 2015). These findings suggest that MAT might be less dependent on PPAR γ or able to adopt alternative differentiation when PPAR γ is absent or inhibited. In fact, a recent publication reported a secondary adipogenic pathway in lipodystrophic 'fat-free' mice (Zhang *et al.*, 2021). Lastly, our preliminary examination of old *Ogt* cKO mice revealed the resolution of BM adiposity, indicating that PPAR γ and its O-GlcNAc modification become essential for the adipogenic differentiation of adult BMSCs.

Protein O-GlcNAcylation senses glucose availability (Hardivillé and Hart, 2014; Ruan *et al.*, 2012), hormonal cues (Ruan *et al.*, 2014; Ruan *et al.*, 2017; Whelan *et al.*, 2008), cellular stress (Martinez *et al.*, 2017; Ruan *et al.*, 2017), and immune signals (Chang *et al.*, 2020; Liu *et al.*, 2019; Zhao *et al.*, 2020; Zhao *et al.*, 2022) to maintain cellular and tissue homeostasis. Osteogenic differentiation of mesenchymal cells induces global O-GlcNAc levels (Kim *et al.*, 2007; Nagel and Ball, 2014); however, the upstream mechanistic regulators of osteoblastic O-GlcNAcylation remain enigmatic. High glucose has been shown to promote O-GlcNAcylation and osteogenic differentiation of cartilage endplate stem cells (Sun *et al.*, 2019). BMSCs preferentially use glycolysis for bioenergetics to support their self-renewal and multipotency (Ito and Suda, 2014; van Gestel and Carmeliet, 2021). Active aerobic glycolysis also fuels the high anabolic demand during bone formation. It would be important in the future to determine whether flux of the hexosamine biosynthetic pathway, a branch of glycolysis (Ruan *et al.*, 2013b), increases to provide more UDP-GlcNAc for O-GlcNAc modification. We also showed here that PTH treatment increased protein O-GlcNAcylation. Signaling through the PTH receptor activates the cAMP-protein kinase A (PKA)-CREB pathway and the accumulation of inositol trisphosphate (IP3) and diacylglycerol (DAG), which further increase intracellular Ca²⁺ and PKC, respectively (Datta and Abou-Samra, 2009). Future experiments are required to determine if OGT enzymatic activity can be regulated by these signaling nodes, for example Ca²⁺/calmodulin-dependent protein kinase II (CaMKII) (Ruan *et al.*, 2017). Sex differences in skeletal development, maintenance, and aging have been well appreciated. Whether BMSC O-GlcNAc signaling is differentially regulated between male and female animals, particularly during puberty and aging, is an important question that remains unaddressed. Since only male mice were investigated in the current study, it is unclear if the reciprocal regulation of RUNX2 and PPAR γ by O-GlcNAcylation in determining the bone-fat balance is equally vital in females.

The BM microenvironment, composed of BMSCs, osteoblasts, adipocytes, sympathetic nerves, and vascular endothelial cells, has been highlighted as an important extrinsic factor for the maintenance and differentiation of distinct hematopoietic lineage progenitors (Bianco and Robey, 2015; Calvi and Link, 2015; Morrison and Scadden, 2014; Wei and Frenette, 2018). While the concomitant development, remodeling, and aging of the skeletal and hematopoietic systems have been observed in various pathophysiological conditions, mechanisms underlying the coordinated regulation of the two systems are less understood. Our current study has provided the first evidence that RUNX2, permitted by O-GlcNAcylation, not only is indispensable for the osteoblast development, but also establishes the endosteal niche for B lymphocytes by driving IL-7 expression (Figure 7). When OGT is deficient, the perivascular BMSCs are prone to adipogenic differentiation, which also activates

C/EBP β -dependent SCF expression and myelopoiesis. During aging, the parallel dysfunction of the skeletal and hematopoietic systems leads to osteoporosis, marrow fat accumulation, and myeloid hematopoietic skewing (Geiger et al., 2013). Whether BMSC aging is associated with O-GlcNAc decline and whether the balance between RUNX and C/EBP β leads to bone-fat imbalances and niche dysfunction require future investigations.

Methods

Key resources table

Reagent type (species) or resource	Designation	Source or reference	Identifiers	Additional information
Genetic reagent (<i>Mus musculus</i>)	<i>Sp7^{GFP:Cre} (B6.Cg-Tg(Sp7-tTA,tetO-EGFP/cre)1Amc/J)</i>	Jackson Laboratory	RRID:IMSR_JAX:006361	
Genetic reagent (<i>Mus musculus</i>)	<i>Ogt^{fl/fl} (B6.129-Ogttm1Gwh/J)</i>	Jackson Laboratory	RRID:IMSR_JAX:004860	
Cell line (<i>Mus musculus</i>)	Primary BMSC	This paper		From long bones of mouse
Cell line (<i>Mus musculus</i>)	C3H10T1/2	ATCC	CCL-226	Verified by ATCC and tested negative for mycoplasma
Cell line (<i>Homo sapiens</i>)	HEK293FT	Invitrogen	R70007	Verified by Invitrogen and tested negative for mycoplasma
Cell line (<i>Cercopithecus aethiops</i>)	COS7	ATCC	CRL-1651	Verified by ATCC and tested negative for mycoplasma
Transfected construct (<i>Mus musculus</i>)	6xOSE2-luc	Phimphilai et al., 2006		
Transfected construct (<i>Renilla reniformis</i>)	pGL4-hRluc	Promega	#E688A	
Transfected construct (<i>Mus musculus</i>)	PPREx3-TK-luc	Addgene	#1015	
Antibody	Anti-Perilipin (Rabbit monoclonal)	Cell Signaling Technology	9349T	IF(1:200)
Antibody	Anti-B220 (Rat monoclonal)	Life Technologies	67-0452-82	FC(1:200)
Antibody	Anti-CD43 (Rat monoclonal)	BD Biosciences	553271	FC(1:200)
Antibody	Anti-CD24 (Rat monoclonal)	Biolegend	101822	FC(1:1000)
Antibody	Anti-Ly-51 (Rat monoclonal)	Biolegend	108305	FC(1:200)
Antibody	Anti-CD127 (Rat monoclonal)	Tonbo Biosciences	20-1271 U100	FC(1:200)
Antibody	Anti-CD25 (Rat monoclonal)	Life Technologies	63-0251-82	FC(1:200)
Antibody	Anti-CD19 (Rat monoclonal)	Biolegend	115545	FC(1:200)
Antibody	Biotin-conjugated lineage antibodies (Rat monoclonal)	Biolegend	133307	FC(1:200)
Antibody	Anti-CD4 (Rat monoclonal)	Biolegend	100403	FC(1:200)
Antibody	Anti-CD5 (Rat monoclonal)	Biolegend	100603	FC(1:200)
Antibody	Anti-CD8 (Rat monoclonal)	Biolegend	100703	FC(1:200)
Antibody	Anti-CD127-APC (Rat monoclonal)	eBioscience	17-1271-82	FC(1:100)
Antibody	Anti-c-Kit-APC-eFluor780 (Rat monoclonal)	eBioscience	47-1171-82	FC(1:400)

Continued on next page

Continued

Reagent type (species) or resource	Designation	Source or reference	Identifiers	Additional information
Antibody	Anti-Sca-1-Super Bright 436 (Rat monoclonal)	eBioscience	62-5981-82	FC(1:100)
Antibody	Anti-CD34-PE (Rat monoclonal)	Biologend	152204	FC(1:100)
Antibody	Anti-FcγR-PerCP-eFluor710 (Rat monoclonal)	eBioscience	46-0161-80	FC(1:400)
Antibody	Anti-CD150-BV605 (Rat monoclonal)	Biologend	115927	FC(1:100)
Antibody	Anti-CD48-BUV395 (Rat monoclonal)	BD Biosciences	740236	FC(1:100)
Antibody	Anti-CD45-BUV395 (Rat monoclonal)	BD Biosciences	564279	FC(1:400)
Antibody	Anti-Ter119-BV421 (Rat monoclonal)	Biologend	116234	FC(1:400)
Antibody	Anti-CD31-BV421 (Rat monoclonal)	Biologend	102424	FC(1:400)
Antibody	Anti-PDGFRα-Super Bright 600 (Rat monoclonal)	eBioscience	63-1401-82	FC(1:100)
Antibody	Anti-VCAM1-PE (Rat monoclonal)	Biologend	105713	FC(1:100)
Recombinant DNA reagent	RUNX2-WT	This paper	pLV-EF1a-RUNX2-WT-IRES-Hygro	See Methods; available upon request
Recombinant DNA reagent	RUNX2-3A/ RUNX2-3SA	This paper	pLV-EF1a-RUNX2-3Mut-IRES-Hygro	See Methods; available upon request
Recombinant DNA reagent	PPAR λ 2-WT	This paper	pLVX- PPAR λ 2-WT-Puro	See Methods; available upon request
Recombinant DNA reagent	PPAR λ 2-T84A	This paper	pLVX- PPAR λ 2-T84A-Puro	See Methods; available upon request
Recombinant DNA reagent	PPAR λ 2-4A	This paper	pLVX- PPAR λ 2-4A-Puro	See Methods; available upon request
Recombinant DNA reagent	PPAR λ 2-5A	This paper	pLVX- PPAR λ 2-5A-Puro	See Methods; available upon request
Recombinant DNA reagent	C/EBPβ-WT	This paper	pCDH-CMV-Cebpb-WT-P2a-Puro	See Methods; available upon request
Recombinant DNA reagent	C/EBPβ-2A	This paper	pCDH-CMV-Cebpb-2MUT-P2a-Puro	See Methods; available upon request
Commercial assay or kit	Q5 Site-Directed Mutagenesis Kit	NEB	#E0554	
Commercial assay or kit	Dual-Luciferase Assay System	Promega	E1910	
Commercial assay or kit	Transporter 5 Transfection Reagent	Polysciences	26008-1 A	
Chemical compound, drug	Parathyroid hormone (PTH)	Genscript	RP01001	
Chemical compound, drug	OSMI-1	Sigma	SML1621-5MG	
Chemical compound, drug	Thiamet-G (TMG)	Biosynth	MD08856	
Chemical compound, drug	Doxycycline food	Bio-Serv	S3888	
Chemical compound, drug	IBMX	CAYMAN	13347	
Chemical compound, drug	Dexamethasone	Sigma	D4902	

Continued on next page

Continued

Reagent type (species) or resource	Designation	Source or reference	Identifiers	Additional information
Chemical compound, drug	Insulin	Sigma	91077 C	
Chemical compound, drug	Rosiglitazone	Sigma	R2408-10MG	
Chemical compound, drug	Ascorbic acid	Sigma	A4403-100MG	
Chemical compound, drug	β -Glycerophosphate	Santa cruz	sc-220452	
Software, algorithm	FlowJ	BD Life Sciences	V10	

Animals

All animal experiments were approved by the institutional animal care and use committee of the University of Minnesota (protocol # 2112–39682 A). All the mice were group-housed in light/dark cycle- (6am–8pm light), temperature- (21.5 ± 1.5 °C), and humidity-controlled (30–70%) room, and had free access to water and regular chow (Teklad #2018) unless otherwise indicated. Moist food was provided to constitutive $Sp7^{GFP:Cre}$ animals to circumvent tooth defects and prevent malnutrition. All mice were maintained on a C57BL6 background. Due to the X-chromosome localization of the *Ogt* gene, only male mice were used in the study if not specified in the text or figures. To suppress Cre activity, designated breeders were fed a diet containing 200 mg/kg doxycycline (Bio-serv, S3888).

BMSC isolation, culture, and differentiation

BMSC were isolated from the long bones as described previously (Zhu *et al.*, 2010). The fragments of long bones were digested with collagenase II for 30 min. The released cells were discarded, and the digested bone fragments were cultivated in the BMSCs growth medium (alpha-MEM supplemented with 10% FBS). Once confluent, cells were switched to either adipogenic differentiation medium (alpha-MEM supplemented with 20% FBS, 500 μ M IBMX, 1 μ M Dexamethasone, 10 μ g/ml Insulin and 1 μ M Rosiglitazone) for the first 2 days. The medium was then changed to adipocyte differentiation base medium (α -MEM supplemented with 20% FBS, 10 μ g/ml Insulin and 1 μ M Rosiglitazone) for the next 4 days followed by oil red O staining. For osteogenic differentiation, cells were induced with osteoblast differentiation medium (α -MEM supplemented with 10% FBS, 0.3 mM ascorbic acid, 10 mM β -glycerophosphate, 0.1 μ M Dexamethasone) for 14 days followed by ALP staining or for 28 days followed by Alizarin red staining.

Cell culture, plasmids, and lentiviruses

HEK 293, COS7, and C3H10T1/2 (ATCC, CCL-226) cells were cultured with DMEM plus 10% of FBS. The mouse RUNX2-Myc/DDK plasmid was purchased from OriGene (MR227321), then subcloned into pLV-EF1a-IRES-Hygro (Addgene #85134). Mouse PPAR γ 2 with a N-terminal MYC tag was subcloned into pLVX-Dsred-puro plasmid. C/EBP β plasmids were kindly provided by Dr. Xiaoyong Yang at Yale University and then subcloned into pCDH-CMV-P2a-Puro. O-GlcNAc sites were mutated into alanine with Q5 Site-Directed Mutagenesis Kit (NEB#E0554). Lentivirus was packed as previously described (Huang *et al.*, 2022). Briefly, 293 FT cells were transfected with over-expression plasmids pSPAX2, and pMD2.G. Media with lentivirus were filtered and added into C3H10T1/2 cells. Seventy-two hr after infection, cells were then selected with drugs according to the resistance genes they possessed.

Luciferase assay

For Runx2 luciferase assay, empty or RUNX2 vectors were transfected into COS7 cells with Lipofectamine, together with 6xOSE2-luc (Phimphilai *et al.*, 2006) and pGL4-hRLuc vectors in which either firefly or Renilla luciferase genes were expressed under the control of the RUNX2-specific or the constitutive SV40 promoter, respectively. After 6 hr, cells were washed three times and with the addition of 50 μ M OSMI-1. Cells were incubated for an additional 48 hr in growth medium containing 5% serum. Luminescent signals were generated using the Dual-Luciferase Assay System (Promega). Relative light units (RLU) for the 6xOSE2 reporter were normalized against pGL4-hRLuc values as an internal control for transfection efficiency. For PPAR γ 2 luciferase assays, C3H10T1/2 cells were

transfected with Transporter 5 Transfection Reagent (Polysciences) following manufacture's protocol. PPAR γ 2 transcriptional activity was determined using the PPREx3-TK-luc reporter (Addgene, #1015).

Histology

Bone tissues were fixed in formalin solution at 4 °C for 24 hr. Tissue embedding, sectioning, and hematoxylin and eosin staining were performed at the Comparative Pathology Shared Resource of the University of Minnesota. For immunostaining, the tissues were embedded in OCT then cut into 7 μ m slides. After three times of PBS wash, the slides were incubated with blocking buffer (3% BSA in PBS) for 1 hr, then immersed with anti-Perilipin (Cell Signaling Technology, #9349) antibody overnight at 4 °C. For immunofluorescence, PBS-washed slides were incubated with a fluorescent secondary antibody at room temperature for 1 hr, and then mounted with VECTASHIELD Antifade Mounting Medium with DAPI after three times of PBS wash. A Nikon system was used for imaging. Goldner's trichrome and Safranin O staining were performed at Servicebio, China.

micro-CT

The samples were scanned with an in vitro micro-CT device (Skyscan 1272, Bruker micro-CT) with scanning parameters of: Source Voltage = 60 kV, Source Current = 166 μ A, exposure 897ms/frame, average of 3 frames per projection, Rotation Step (deg)=0.200 and 0.25 mm Aluminum filter. The specimens were scanned at high resolution (2016 \times 1344 pixels) with an Isotropic voxel size of 7.1 μ m. Reconstructions for X-ray projections and re-alignment were performed using the Skyscan software (NRecon and DataViewer) (v. 1.7.3.1, Brüker micro-CT, Kontich, Belgium). Ring artefact and beam hardening corrections were applied in reconstruction. Datasets were loaded into SkyScan CT-Analyzer software for measurement of BMD. Calibration was performed with 0.25- and 0.75 mg/mL hydroxyapatite mice phantoms provided by SkyScan. For cancellous and cortical bone analysis, the scanning regions were confined to the distal metaphysis, 100 slices starting at 0.5 mm proximally from the proximal tip of the primary spongiosa for the cancellous portion and 100 slices starting at 4.5 mm proximally from the center of intercondylar fossa for the cortical portion.

O-GlcNAc mass spectrometry

Myc-tagged PPAR γ 2 was co-transfected with OGT into 15 cm-dishes of 293T cells and purified by immunoprecipitation with anti-c-Myc agarose beads (Pierce), followed by PAGE gel electrophoresis. The corresponding PPAR γ 2 band was cut for in gel Trypsin (Promega) digestion. Tryptic peptides were analyzed by on-line LC-MS/MS using an Orbitrap Fusion Lumos (Thermo) coupled with a NanoAcquity UPLC system (Waters) as we previously reported (Liu *et al.*, 2019; Zhao *et al.*, 2022). Peaklists were generated using PAVA (UCSF) and searched using Protein Prospector 5.23.0 against the SwissProt database and a randomized concatenated database with the addition of the recombinant PPAR γ 2 sequence. HexNAcylated peptides were manually verified.

Real-time RT-PCR

RNA was isolated with Trizol and reverse transcribed into cDNA with the iScript cDNA Synthesis Kit. Real-time RT-PCR was performed using iTaq Universal SYBR Green Supermix and gene-specific primers (Figure 6—source data 1) on a Bio-Rad C1000 Thermal Cycler.

Flow cytometry

For PDGFR α +VCAM1+preadipocytes, BM cells were stained with anti-CD45, anti-Ter119, anti-CD31, anti-PDGFR α , and anti-VCAM1. We gated the PDGFR α +VCAM1+ cells after excluding the CD45+Ter119+CD31+ cells. For B-cell lymphopoiesis, BM cells were stained in PBS containing 1% (w/v) bovine serum albumin on ice for 30 min, with anti-B220 (Life Technologies, 67-0452-82), anti-CD43 (BD Biosciences, 553271), anti-CD24 (Biolegend, 101822), anti-Ly-51 (Biolegend, 108305), anti-CD127 (Tonbo Biosciences, 20–1271 U100), anti-CD25 (Life Technologies, 63-0251-82) and anti-CD19 (Biolegend, 115545). For hematopoietic stem and progenitor cells, BM cells were stained with a cocktail of biotin-conjugated lineage antibodies CD3e, B220, Ter119, Mac-1 and Gr-1 (Biolegend, 133307), CD4 (Biolegend, 100403), CD5 (Biolegend, 100603), CD8 (Biolegend, 100703), followed by Streptavidin-AF488 (Biolegend, 405235). Cells were then stained with CD127-APC (eBioscience, 17-1271-82), c-Kit-APC-eFluor780 (eBioscience, 47-1171-82), Sca-1-Super Bright 436 (eBioscience, 62-5981-82),

CD34-PE (Biolegend, 152204) and FcyR-PerCP-eFluor710 (eBioscience, 46-0161-80), CD150-BV605 (Biolegend, 115927), and CD48-BUV395 (BDBioscience, 740236). Fixable Viability Dye was used to exclude dead cells as instructed by the manufacturer. A complete list of used antibodies was shown in **Figure 5—source data 1**. Flow cytometry was performed on an LSR Fortessa H0081 or X20 and analyzed with FlowJo.

Quantification and statistical analysis

Results are shown as mean \pm SEM. N values (biological replicates) and statistical analysis methods are described in figure legends. The statistical comparisons were carried out using two-tailed unpaired Student's t-test and one-way or two-way ANOVA with indicated post hoc tests with Prism 9 (Graphpad). Differences were considered significant when $p < 0.05$; *, $p < 0.05$; **, $p < 0.01$; ***, $p < 0.001$.

Acknowledgements

We thank Dr. Xiaoyong Yang for kindly providing wildtype and mutant C/EBP β plasmids; Dr. Renny Franchesci for providing the 6xOSE2-luc plasmid; and Alexis Nagel for Runx2 luciferase assay. This work was supported by the National Natural Science Foundation of China, China (32170847) to ZH, NIH/NIAID (R01 AI162678) to HZ, the Miriam and Sheldon G Adelson Medical Research Foundation to JCM and ALB, and NIH/NIAID (R01 AI139420 and R01 AI162791) to H-BR.

Additional information

Funding

Funder	Grant reference number	Author
National Natural Science Foundation of China	32170847	Zan Huang
National Institutes of Health	R01 AI162678	Hu Zeng
National Institutes of Health	R01 AI139420	Hai-Bin Ruan
National Institutes of Health	R01 AI162791	Hai-Bin Ruan
Dr. Miriam and Sheldon G. Adelson Medical Research Foundation		Jason C Maynard Alma L Burlingame

The funders had no role in study design, data collection and interpretation, or the decision to submit the work for publication.

Author contributions

Zengdi Zhang, Formal analysis, Investigation, Methodology, Writing - original draft; Zan Huang, Formal analysis, Funding acquisition, Investigation, Methodology, Writing - original draft; Mohamed Awad, Jason C Maynard, Data curation, Investigation, Methodology; Mohammed Elsalanty, Supervision, Methodology; James Cray, Resources, Methodology; Lauren E Ball, Investigation; Alma L Burlingame, Kim C Mansky, Resources, Supervision; Hu Zeng, Supervision, Funding acquisition, Investigation; Hai-Bin Ruan, Conceptualization, Resources, Supervision, Funding acquisition, Writing - original draft, Writing - review and editing

Author ORCIDs

Hai-Bin Ruan  <http://orcid.org/0000-0002-3858-1272>

Ethics

All animal experiments were approved by the institutional animal care and use committee of the University of Minnesota (protocol # 2112-39682A).

Decision letter and Author responseDecision letter <https://doi.org/10.7554/eLife.85464.sa1>Author response <https://doi.org/10.7554/eLife.85464.sa2>

Additional files**Supplementary files**

- MDAR checklist

Data availability

All data generated or analyzed during this study are included in the manuscript and supporting file. Supplementary tables have been provided for Mass spectrometry, primer sequences, and antibody list.

References

- Aaron N, Kraakman MJ, Zhou Q, Liu Q, Costa S, Yang J, Liu L, Yu L, Wang L, He Y, Fan L, Hirakawa H, Ding L, Lo J, Wang W, Zhao B, Guo E, Sun L, Rosen CJ, Qiang L. 2021. Adipsin promotes bone marrow adiposity by priming mesenchymal stem cells. *eLife* **10**:e69209. DOI: <https://doi.org/10.7554/eLife.69209>, PMID: 34155972
- Ahrends R, Ota A, Kovary KM, Kudo T, Park BO, Teruel MN. 2014. Controlling low rates of cell differentiation through noise and ultrahigh feedback. *Science* **344**:1384–1389. DOI: <https://doi.org/10.1126/science.1252079>, PMID: 24948735
- Ambrosi TH, Scialdone A, Graja A, Gohlke S, Jank AM, Bocian C, Woelk L, Fan H, Logan DW, Schürmann A, Saraiva LR, Schulz TJ. 2017. Adipocyte accumulation in the bone marrow during obesity and aging impairs stem cell-based hematopoietic and bone regeneration. *Cell Stem Cell* **20**:771–784. DOI: <https://doi.org/10.1016/j.stem.2017.02.009>, PMID: 28330582
- Ambrosi TH, Longaker MT, Chan CKF. 2019. A revised perspective of skeletal stem cell biology. *Frontiers in Cell and Developmental Biology* **7**:189. DOI: <https://doi.org/10.3389/fcell.2019.00189>, PMID: 31572721
- Andrés-Bergós J, Tardio L, Larranaga-Vera A, Gómez R, Herrero-Beaumont G, Largo R. 2012. The increase in O-linked N-acetylglucosamine protein modification stimulates chondrogenic differentiation both in vitro and in vivo. *The Journal of Biological Chemistry* **287**:33615–33628. DOI: <https://doi.org/10.1074/jbc.M112.354241>, PMID: 22859309
- Asada N, Kunisaki Y, Pierce H, Wang Z, Fernandez NF, Birbrair A, Ma'ayan A, Frenette PS. 2017. Differential cytokine contributions of perivascular haematopoietic stem cell niches. *Nature Cell Biology* **19**:214–223. DOI: <https://doi.org/10.1038/ncb3475>, PMID: 28218906
- Baryawno N, Przybylski D, Kowalczyk MS, Kfoury Y, Severe N, Gustafsson K, Kokkalis KD, Mercier F, Tabaka M, Hofree M, Dionne D, Papazian A, Lee D, Ashenberg O, Subramanian A, Vaishnav ED, Rozenblatt-Rosen O, Regev A, Scadden DT. 2019. A cellular taxonomy of the bone marrow stroma in homeostasis and leukemia. *Cell* **177**:1915–1932. DOI: <https://doi.org/10.1016/j.cell.2019.04.040>, PMID: 31130381
- Bethel M, Chitteti BR, Srour EF, Kacena MA. 2013. The changing balance between osteoblastogenesis and adipogenesis in aging and its impact on hematopoiesis. *Current Osteoporosis Reports* **11**:99–106. DOI: <https://doi.org/10.1007/s11914-013-0135-6>, PMID: 23423562
- Bianco P, Robey PG. 2015. Skeletal stem cells. *Development* **142**:1023–1027. DOI: <https://doi.org/10.1242/dev.102210>, PMID: 25758217
- Brunmeir R, Xu F. 2018. Functional regulation of PPARs through post-translational modifications. *International Journal of Molecular Sciences* **19**:1738. DOI: <https://doi.org/10.3390/ijms19061738>, PMID: 29895749
- Calvi LM, Link DC. 2015. The hematopoietic stem cell niche in homeostasis and disease. *Blood* **126**:2443–2451. DOI: <https://doi.org/10.1182/blood-2015-07-533588>, PMID: 26468230
- Cao Z, Umek RM, McKnight SL. 1991. Regulated expression of three C/EBP isoforms during adipose conversion of 3T3-L1 cells. *Genes & Development* **5**:1538–1552. DOI: <https://doi.org/10.1101/gad.5.9.1538>, PMID: 1840554
- Chang YH, Weng CL, Lin KI. 2020. O-glcNacylation and its role in the immune system. *Journal of Biomedical Science* **27**:57. DOI: <https://doi.org/10.1186/s12929-020-00648-9>, PMID: 32349769
- Chen J, Shi Y, Regan J, Karuppaiah K, Ornitz DM, Long F. 2014. Osx-cre targets multiple cell types besides osteoblast lineage in postnatal mice. *PLOS ONE* **9**:e85161. DOI: <https://doi.org/10.1371/journal.pone.0085161>
- Chen Y, Zhao X, Wu H. 2021. Transcriptional programming in arteriosclerotic disease: A multifaceted function of the runx2 (runt-related transcription factor 2). *Arteriosclerosis, Thrombosis, and Vascular Biology* **41**:20–34. DOI: <https://doi.org/10.1161/ATVBAHA.120.313791>, PMID: 33115268
- Cordeiro Gomes A, Hara T, Lim VY, Herndler-Brandstetter D, Nevius E, Sugiyama T, Tani-Ichi S, Schlenner S, Richie E, Rodewald H-R, Flavell RA, Nagasawa T, Ikuta K, Pereira JP. 2016. Hematopoietic stem cell niches produce lineage-instructive signals to control multipotent progenitor differentiation. *Immunity* **45**:1219–1231. DOI: <https://doi.org/10.1016/j.immuni.2016.11.004>, PMID: 27913094

- Darlington GJ**, Ross SE, MacDougald OA. 1998. The role of C/EBP genes in adipocyte differentiation. *The Journal of Biological Chemistry* **273**:30057–30060. DOI: <https://doi.org/10.1074/jbc.273.46.30057>, PMID: 9804754
- Datta NS**, Abou-Samra AB. 2009. PTH and pthrp signaling in osteoblasts. *Cellular Signalling* **21**:1245–1254. DOI: <https://doi.org/10.1016/j.cellsig.2009.02.012>, PMID: 19249350
- Ding L**, Saunders TL, Enikolopov G, Morrison SJ. 2012. Endothelial and perivascular cells maintain haematopoietic stem cells. *Nature* **481**:457–462. DOI: <https://doi.org/10.1038/nature10783>, PMID: 22281595
- Dolgalev I**, Tikhonova AN. 2021. Connecting the dots: Resolving the bone marrow niche heterogeneity. *Frontiers in Cell and Developmental Biology* **9**:622519. DOI: <https://doi.org/10.3389/fcell.2021.622519>, PMID: 33777933
- Fazeli PK**, Horowitz MC, MacDougald OA, Scheller EL, Rodeheffer MS, Rosen CJ, Klibanski A. 2013. Marrow fat and bone -- new perspectives. *The Journal of Clinical Endocrinology and Metabolism* **98**:935–945. DOI: <https://doi.org/10.1210/jc.2012-3634>, PMID: 23393168
- Fistonich C**, Zehentmeier S, Bednarski JJ, Miao R, Schjerven H, Sleckman BP, Pereira JP. 2018. Cell circuits between B cell progenitors and IL-7+ mesenchymal progenitor cells control B cell development. *The Journal of Experimental Medicine* **215**:2586–2599. DOI: <https://doi.org/10.1084/jem.20180778>, PMID: 30158115
- Geiger H**, de Haan G, Florian MC. 2013. The ageing haematopoietic stem cell compartment. *Nature Reviews. Immunology* **13**:376–389. DOI: <https://doi.org/10.1038/nri3433>, PMID: 23584423
- Hanover JA**, Krause MW, Love DC. 2012. Bittersweet memories: Linking metabolism to epigenetics through O-GlcNAcylation. *Nature Reviews. Molecular Cell Biology* **13**:312–321. DOI: <https://doi.org/10.1038/nrm3334>, PMID: 22522719
- Hardivillé S**, Hart GW. 2014. Nutrient regulation of signaling, transcription, and cell physiology by O-GlcNAcylation. *Cell Metabolism* **20**:208–213. DOI: <https://doi.org/10.1016/j.cmet.2014.07.014>, PMID: 25100062
- Hardy RR**, Carmack CE, Shinton SA, Kemp JD, Hayakawa K. 1991. Resolution and characterization of pro-B and pre-pro-B cell stages in normal mouse bone marrow. *The Journal of Experimental Medicine* **173**:1213–1225. DOI: <https://doi.org/10.1084/jem.173.5.1213>, PMID: 1827140
- Hart GW**, Housley MP, Slawson C. 2007. Cycling of O-linked beta-N-acetylglucosamine on nucleocytoplasmic proteins. *Nature* **446**:1017–1022. DOI: <https://doi.org/10.1038/nature05815>, PMID: 17460662
- Ho Y-H**, Del Toro R, Rivera-Torres J, Rak J, Korn C, García-García A, Macías D, González-Gómez C, Del Monte A, Wittner M, Waller AK, Foster HR, López-Otín C, Johnson RS, Nerlov C, Ghevaert C, Vainchenker W, Louache F, Andrés V, Méndez-Ferrer S. 2019. Remodeling of bone marrow hematopoietic stem cell niches promotes myeloid cell expansion during premature or physiological aging. *Cell Stem Cell* **25**:407–418. DOI: <https://doi.org/10.1016/j.stem.2019.06.007>, PMID: 31303548
- Huang Z**, Zhang Z, Moazzami Z, Heck R, Hu P, Nanda H, Ren K, Sun Z, Bartolomucci A, Gao Y, Chung D, Zhu W, Shen S, Ruan HB. 2022. Brown adipose tissue involution associated with progressive restriction in progenitor competence. *Cell Reports* **39**:110575. DOI: <https://doi.org/10.1016/j.celrep.2022.110575>, PMID: 35417710
- Ito K**, Suda T. 2014. Metabolic requirements for the maintenance of self-renewing stem cells. *Nature Reviews. Molecular Cell Biology* **15**:243–256. DOI: <https://doi.org/10.1038/nrm3772>, PMID: 24651542
- Ji S**, Park SY, Roth J, Kim HS, Cho JW. 2012. O-Glcnc modification of PPAR γ reduces its transcriptional activity. *Biochemical and Biophysical Research Communications* **417**:1158–1163. DOI: <https://doi.org/10.1016/j.bbrc.2011.12.086>, PMID: 22226965
- Kajkenova O**, Lecka-Czernik B, Gubrij I, Hauser SP, Takahashi K, Parfitt AM, Jilka RL, Manolagas SC, Lipschitz DA. 1997. Increased adipogenesis and myelopoiesis in the bone marrow of SAMP6, a murine model of defective osteoblastogenesis and low turnover osteopenia. *Journal of Bone and Mineral Research* **12**:1772–1779. DOI: <https://doi.org/10.1359/jbmr.1997.12.11.1772>, PMID: 9383681
- Kim SH**, Kim YH, Song M, An SH, Byun HY, Heo K, Lim S, Oh YS, Ryu SH, Suh PG. 2007. O-Glcnc modification modulates the expression of osteocalcin via OSE2 and Runx2. *Biochemical and Biophysical Research Communications* **362**:325–329. DOI: <https://doi.org/10.1016/j.bbrc.2007.07.149>, PMID: 17707335
- Kim WJ**, Shin HL, Kim BS, Kim HJ, Ryoo HM. 2020. RUNX2-modifying enzymes: Therapeutic targets for bone diseases. *Experimental & Molecular Medicine* **52**:1178–1184. DOI: <https://doi.org/10.1038/s12276-020-0471-4>, PMID: 32788656
- Kobayashi T**, Kronenberg HM. 2021. Overview of skeletal development. *Methods in Molecular Biology* **2230**:3–16. DOI: https://doi.org/10.1007/978-1-0716-1028-2_1, PMID: 33197005
- Komori T**, Yagi H, Nomura S, Yamaguchi A, Sasaki K, Deguchi K, Shimizu Y, Bronson RT, Gao YH, Inada M, Sato M, Okamoto R, Kitamura Y, Yoshiki S, Kishimoto T. 1997. Targeted disruption of cbfa1 results in a complete lack of bone formation owing to maturational arrest of osteoblasts. *Cell* **89**:755–764. DOI: [https://doi.org/10.1016/s0092-8674\(00\)80258-5](https://doi.org/10.1016/s0092-8674(00)80258-5), PMID: 9182763
- Krishnan V**, Moore TL, Ma YL, Helvering LM, Frolik CA, Valasek KM, Ducy P, Geiser AG. 2003. Parathyroid hormone bone anabolic action requires cbfa1/runx2-dependent signaling. *Molecular Endocrinology* **17**:423–435. DOI: <https://doi.org/10.1210/me.2002-0225>, PMID: 12554794
- Li X**, Molina H, Huang H, Zhang Y-Y, Liu M, Qian S-W, Slawson C, Dias WB, Pandey A, Hart GW, Lane MD, Tang Q-Q. 2009. O-linked N-acetylglucosamine modification on CCAAT enhancer-binding protein beta: role during adipocyte differentiation. *The Journal of Biological Chemistry* **284**:19248–19254. DOI: <https://doi.org/10.1074/jbc.M109.005678>, PMID: 19478079
- Liu Y**, Strecker S, Wang L, Kronenberg MS, Wang W, Rowe DW, Maye P. 2013. Osterix-cre labeled progenitor cells contribute to the formation and maintenance of the bone marrow stroma. *PLOS ONE* **8**:e71318. DOI: <https://doi.org/10.1371/journal.pone.0071318>, PMID: 23951132

- Liu H**, Xia X, Li B. 2015. Mesenchymal stem cell aging: Mechanisms and influences on skeletal and non-skeletal tissues. *Experimental Biology and Medicine* **240**:1099–1106. DOI: <https://doi.org/10.1177/1535370215591828>, PMID: 26088863
- Liu B**, Salgado OC, Singh S, Hippen KL, Maynard JC, Burlingame AL, Ball LE, Blazar BR, Farrar MA, Hogquist KA, Ruan HB. 2019. The lineage stability and suppressive program of regulatory T cells require protein O-glycosylation. *Nature Communications* **10**:354. DOI: <https://doi.org/10.1038/s41467-019-08300-3>, PMID: 30664665
- Maes C**, Kobayashi T, Selig MK, Torrekens S, Roth SI, Mackem S, Carmeliet G, Kronenberg HM. 2010. Osteoblast precursors, but not mature osteoblasts, move into developing and fractured bones along with invading blood vessels. *Developmental Cell* **19**:329–344. DOI: <https://doi.org/10.1016/j.devcel.2010.07.010>, PMID: 20708594
- Martinez MR**, Dias TB, Natov PS, Zachara NE. 2017. Stress-Induced O-GlcNAcylation: an adaptive process of injured cells. *Biochemical Society Transactions* **45**:237–249. DOI: <https://doi.org/10.1042/BST20160153>, PMID: 28202678
- Mizoguchi T**, Pinho S, Ahmed J, Kunisaki Y, Hanoun M, Mendelson A, Ono N, Kronenberg HM, Frenette PS. 2014. Osterix marks distinct waves of primitive and definitive stromal progenitors during bone marrow development. *Developmental Cell* **29**:340–349. DOI: <https://doi.org/10.1016/j.devcel.2014.03.013>, PMID: 24823377
- Morrison SJ**, Scadden DT. 2014. The bone marrow niche for haematopoietic stem cells. *Nature* **505**:327–334. DOI: <https://doi.org/10.1038/nature12984>, PMID: 24429631
- Nagel AK**, Schilling M, Comte-Walters S, Berkaw MN, Ball LE. 2013. Identification of O-linked N-acetylglucosamine (O-GlcNAc)-modified osteoblast proteins by electron transfer dissociation tandem mass spectrometry reveals proteins critical for bone formation. *Molecular & Cellular Proteomics* **12**:945–955. DOI: <https://doi.org/10.1074/mcp.M112.026633>, PMID: 23443134
- Nagel AK**, Ball LE. 2014. O-GlcNAc modification of the runt-related transcription factor 2 (Runx2) links osteogenesis and nutrient metabolism in bone marrow mesenchymal stem cells. *Molecular & Cellular Proteomics* **13**:3381–3395. DOI: <https://doi.org/10.1074/mcp.M114.040691>, PMID: 25187572
- Ono N**, Ono W, Nagasawa T, Kronenberg HM. 2014. A subset of chondrogenic cells provides early mesenchymal progenitors in growing bones. *Nature Cell Biology* **16**:1157–1167. DOI: <https://doi.org/10.1038/ncb3067>, PMID: 25419849
- Otto F**, Thornell AP, Crompton T, Denzel A, Gilmour KC, Rosewell IR, Stamp GW, Beddington RS, Mundlos S, Olsen BR, Selby PB, Owen MJ. 1997. Cbfa1, a candidate gene for cleidocranial dysplasia syndrome, is essential for osteoblast differentiation and bone development. *Cell* **89**:765–771. DOI: [https://doi.org/10.1016/s0092-8674\(00\)80259-7](https://doi.org/10.1016/s0092-8674(00)80259-7), PMID: 9182764
- Phipphilai M**, Zhao Z, Boules H, Roca H, Franceschi RT. 2006. Bmp signaling is required for Runx2-dependent induction of the osteoblast phenotype. *Journal of Bone and Mineral Research* **21**:637–646. DOI: <https://doi.org/10.1359/jbmr.060109>, PMID: 16598384
- Qian K**, Wang S, Fu M, Zhou J, Singh JP, Li M-D, Yang Y, Zhang K, Wu J, Nie Y, Ruan H-B, Yang X. 2018. Transcriptional regulation of O-GlcNAc homeostasis is disrupted in pancreatic cancer. *The Journal of Biological Chemistry* **293**:13989–14000. DOI: <https://doi.org/10.1074/jbc.RA118.004709>, PMID: 30037904
- Rauch A**, Haakonsson AK, Madsen JGS, Larsen M, Forss I, Madsen MR, Van Hauwaert EL, Wiwie C, Jespersen NZ, Tencerova M, Nielsen R, Larsen BD, Röttger R, Baumbach J, Scheele C, Kassem M, Mandrup S. 2019. Osteogenesis depends on commissioning of a network of stem cell transcription factors that act as repressors of adipogenesis. *Nature Genetics* **51**:716–727. DOI: <https://doi.org/10.1038/s41588-019-0359-1>, PMID: 30833796
- Ruan HB**, Han X, Li MD, Singh JP, Qian K, Azarhoush S, Zhao L, Bennett AM, Samuel VT, Wu J, Yates JR, Yang X. 2012. O-glcnaC transferase/host cell factor C1 complex regulates gluconeogenesis by modulating PGC-1 α stability. *Cell Metabolism* **16**:226–237. DOI: <https://doi.org/10.1016/j.cmet.2012.07.006>, PMID: 22883232
- Ruan HB**, Nie Y, Yang X. 2013a. Regulation of protein degradation by O-glcnaCylation: crosstalk with ubiquitination. *Molecular & Cellular Proteomics* **12**:3489–3497. DOI: <https://doi.org/10.1074/mcp.R113.029751>, PMID: 23824911
- Ruan HB**, Singh JP, Li MD, Wu J, Yang X. 2013b. Cracking the O-glcnaC code in metabolism. *Trends in Endocrinology and Metabolism* **24**:301–309. DOI: <https://doi.org/10.1016/j.tem.2013.02.002>, PMID: 23647930
- Ruan HB**, Dietrich MO, Liu ZW, Zimmer MR, Li MD, Singh JP, Zhang K, Yin R, Wu J, Horvath TL, Yang X. 2014. O-GlcnaC transferase enables AGRP neurons to suppress browning of white fat. *Cell* **159**:306–317. DOI: <https://doi.org/10.1016/j.cell.2014.09.010>, PMID: 25303527
- Ruan H-B**, Ma Y, Torres S, Zhang B, Feriod C, Heck RM, Qian K, Fu M, Li X, Nathanson MH, Bennett AM, Nie Y, Ehrlich BE, Yang X. 2017. Calcium-Dependent O-GlcNAc signaling drives liver autophagy in adaptation to starvation. *Genes & Development* **31**:1655–1665. DOI: <https://doi.org/10.1101/gad.305441.117>, PMID: 28903979
- Scheller EL**, Doucette CR, Learman BS, Cawthorn WP, Khandaker S, Schell B, Wu B, Ding SY, Bredella MA, Fazeli PK, Khoury B, Jepsen KJ, Pilch PF, Klibanski A, Rosen CJ, MacDougald OA. 2015. Region-specific variation in the properties of skeletal adipocytes reveals regulated and constitutive marrow adipose tissues. *Nature Communications* **6**:7808. DOI: <https://doi.org/10.1038/ncomms8808>, PMID: 26245716
- Scheller EL**, Cawthorn WP, Burr AA, Horowitz MC, MacDougald OA. 2016. Marrow adipose tissue: Trimming the fat. *Trends in Endocrinology and Metabolism* **27**:392–403. DOI: <https://doi.org/10.1016/j.tem.2016.03.016>, PMID: 27094502

- Shu HS**, Liu YL, Tang XT, Zhang XS, Zhou B, Zou W, Zhou BO. 2021. Tracing the skeletal progenitor transition during postnatal bone formation. *Cell Stem Cell* **28**:2122–2136. DOI: <https://doi.org/10.1016/j.stem.2021.08.010>, PMID: 34499868
- Singer K**, DelProposto J, Morris DL, Zamarron B, Mergian T, Maley N, Cho KW, Geletka L, Subbaiah P, Muir L, Martinez-Santibanez G, Lumeng CN-K. 2014. Diet-Induced obesity promotes myelopoiesis in hematopoietic stem cells. *Molecular Metabolism* **3**:664–675. DOI: <https://doi.org/10.1016/j.molmet.2014.06.005>, PMID: 25161889
- Sun C**, Lan W, Li B, Zuo R, Xing H, Liu M, Li J, Yao Y, Wu J, Tang Y, Liu H, Zhou Y. 2019. Glucose regulates tissue-specific chondro-osteogenic differentiation of human cartilage endplate stem cells via O-glcNacetylation of SOX9 and runx2. *Stem Cell Research & Therapy* **10**:357. DOI: <https://doi.org/10.1186/s13287-019-1440-5>, PMID: 31779679
- Takarada T**, Nakazato R, Tsuchikane A, Fujikawa K, Iezaki T, Yoneda Y, Hinoi E. 2016. Genetic analysis of runx2 function during intramembranous ossification. *Development* **143**:211–218. DOI: <https://doi.org/10.1242/dev.128793>, PMID: 26657773
- van Gestel N**, Carmeliet G. 2021. Metabolic regulation of skeletal cell fate and function in physiology and disease. *Nature Metabolism* **3**:11–20. DOI: <https://doi.org/10.1038/s42255-020-00321-3>, PMID: 33398192
- Wang L**, Feng J, Deng Y, Yang Q, Wei Q, Ye D, Rong X, Guo J. 2022. Ccaat/enhancer-binding proteins in fibrosis: complex roles beyond conventional understanding. *Research* **2022**:9891689. DOI: <https://doi.org/10.34133/2022/9891689>, PMID: 36299447
- Wei Q**, Frenette PS. 2018. Niches for hematopoietic stem cells and their progeny. *Immunity* **48**:632–648. DOI: <https://doi.org/10.1016/j.immuni.2018.03.024>, PMID: 29669248
- Whelan SA**, Lane MD, Hart GW. 2008. Regulation of the O-linked beta-N-acetylglucosamine transferase by insulin signaling. *The Journal of Biological Chemistry* **283**:21411–21417. DOI: <https://doi.org/10.1074/jbc.M800677200>, PMID: 18519567
- Yang X**, Qian K. 2017. Protein O-GlcNAcylation: Emerging mechanisms and functions. *Nature Reviews. Molecular Cell Biology* **18**:452–465. DOI: <https://doi.org/10.1038/nrm.2017.22>, PMID: 28488703
- Yu VWC**, Lymperi S, Oki T, Jones A, Swiatek P, Vasic R, Ferraro F, Scadden DT. 2016. Distinctive mesenchymal-parenchymal cell pairings govern B cell differentiation in the bone marrow. *Stem Cell Reports* **7**:220–235. DOI: <https://doi.org/10.1016/j.stemcr.2016.06.009>, PMID: 27453006
- Zhang Z**, Huang Z, Ong B, Sahu C, Zeng H, Ruan HB. 2019. Bone marrow adipose tissue-derived stem cell factor mediates metabolic regulation of hematopoiesis. *Haematologica* **104**:1731–1743. DOI: <https://doi.org/10.3324/haematol.2018.205856>, PMID: 30792196
- Zhang X**, Robles H, Magee KL, Lorenz MR, Wang Z, Harris CA, Craft CS, Scheller EL. 2021. A bone-specific adipogenesis pathway in fat-free mice defines key origins and adaptations of bone marrow adipocytes with age and disease. *eLife* **10**:e66275. DOI: <https://doi.org/10.7554/eLife.66275>, PMID: 34378533
- Zhao M**, Ren K, Xiong X, Cheng M, Zhang Z, Huang Z, Han X, Yang X, Alejandro EU, Ruan HB. 2020. Protein O-glcNac modification links dietary and gut microbial cues to the differentiation of enteroendocrine L cells. *Cell Reports* **32**:108013. DOI: <https://doi.org/10.1016/j.celrep.2020.108013>, PMID: 32783937
- Zhao Ming**, Ren K, Xiong X, Xin Y, Zou Y, Maynard JC, Kim A, Battist AP, Koneripalli N, Wang Y, Chen Q, Xin R, Yang C, Huang R, Yu J, Huang Z, Zhang Z, Wang H, Wang D, Xiao Y, et al. 2022. Epithelial STAT6 O-GlcNAcylation drives a concerted anti-helminth alarmin response dependent on tuft cell hyperplasia and gasdermin C. *Immunity* **55**:623–638. DOI: <https://doi.org/10.1016/j.immuni.2022.03.009>, PMID: 35385697
- Zhong L**, Yao L, Tower RJ, Wei Y, Miao Z, Park J, Shrestha R, Wang L, Yu W, Holdreith N, Huang X, Zhang Y, Tong W, Gong Y, Ahn J, Susztak K, Dymont N, Li M, Long F, Chen C, et al. 2020. Single cell transcriptomics identifies a unique adipose lineage cell population that regulates bone marrow environment. *eLife* **9**:e54695. DOI: <https://doi.org/10.7554/eLife.54695>, PMID: 32286228
- Zhou BO**, Yu H, Yue R, Zhao Z, Rios JJ, Naveiras O, Morrison SJ. 2017. Bone marrow adipocytes promote the regeneration of stem cells and haematopoiesis by secreting SCF. *Nature Cell Biology* **19**:891–903. DOI: <https://doi.org/10.1038/ncb3570>, PMID: 28714970
- Zhu H**, Guo ZK, Jiang XX, Li H, Wang XY, Yao HY, Zhang Y, Mao N. 2010. A protocol for isolation and culture of mesenchymal stem cells from mouse compact bone. *Nature Protocols* **5**:550–560. DOI: <https://doi.org/10.1038/nprot.2009.238>, PMID: 20203670